Integrated Nonlinear Structural Simulation of Tall Buildings in Fire

Mhd Anwar Orabi[1], Aatif Ali Khan[1,*], Liming Jiang[1] , Tejeswar Yarlagadda[1], Jose Torero[2], Asif Usmani[1]

[1]*Department of Building Services Engineering, The Hong Kong Polytechnic University, Hong Kong*

[2]*Department of Civil, Environmental & Geomatic Engineering, University College London, London, UK*

ABSTRACT

The collapse of several tall buildings over the last two decades has shown that the performance of tall and complex buildings in fire is a necessary design consideration that ought to go beyond simple code compliance. To this end, several advancements in the field of numerical simulation of both the fire and the thermomechanical response of structures have been made. In isolation, the practical benefit of these advancements is limited, and their true potential is only unlocked when the results of those numerical simulations are integrated. This paper starts by showcasing recent developments in the thermal and thermomechanical analysis of structures using OpenSees. Integration of these developments into a unified simulation environment combining fire simulation, heat transfer, and mechanical analysis is then introduced. Finally, a demonstration example based on the large compartment Cardington experiment is used to showcase the necessity and efficiency of the developed simulation environment for thermomechanical simulation of tall and complex structures in fire.

Keywords –simulation, tall building, fire, CFD, finite element

1. Introduction

Modern architectural designs seek to maximise, when possible, open space within a building, allow for natural light, and improve thermal comfort using natural ventilation and heavily insulated building envelopes. This is particularly the case for office buildings, where tenants occupy large surface areas. These aims produce a more environmentally and occupant friendly built environment, but also introduce a set of hidden but serious fire hazards. Thermally efficient cladding systems, for example, were amongst the factors that led to the tragic and deadly Grenfell Tower disaster [1,2]. The risks posed by these systems are often not fully mitigated, and the resulting fires may grow and spread in uncontrollable ways [3]. Another hidden risk arises from the large open spaces that almost completely alter the fire

behaviour from the well-established small-compartment-focused standard and parametric temperature-time curves [4,5]. In addition to the life hazard these fires present, the risk for structural collapse also increases because of the often unanticipated severe and complex thermo-mechanical response of the structural system.

As the last line of defence against fire, structural resilience is of the utmost importance. As the National Institute of Standards and Technology (NIST) concluded from their investigation of the World Trade Center catastrophe: "fire resistance of structures be enhanced by requiring a performance objective that uncontrolled building fires result in burnout without partial or global (total) collapse." [6]. If this objective is to be met and if tall and complex buildings are to be designed for performance in fire rather than simple code-compliance, then it is necessary to utilise the advanced numerical simulation tools now available [7].

The simulation of structures in fire have progressed in two natural ways: simulation of the fire event, and simulation of the structural response to that event. For the first, computational fluid dynamics (CFD) analysis has emerged as the most prevalent method. Currently, there are many available CFD tools capable of simulating fire behaviour such as OpenFOAM, CFX, and fire dynamics simulator (FDS). FDS is an open-source CFD engine written in FORTRAN by NIST and specialising in the simulation of fire and smoke [8]. Despite being the most prevalent and virtually the industry-standard, FDS has some limitations as will be discussed in first section of the article. For the simulation of building response to the fire event multiple tools also exist. OpenSees is one of these tools which uses the finite element method (FEM) to analyse structural response [9]. Since OpenSees is an open-source project, it was extended for thermomechanical analysis by researchers first at the university of Edinburgh and currently at the Hong Kong Polytechnic University [10–13]. In addition to its mechanical analysis capabilities, OpenSees also includes a heat transfer (HT) module and material library allowing it to also perform 1D through 3D thermal analyses [14].

Unfortunately, because of its academic origin OpenSees grew disproportionately in its capabilities compared to its practicality. While it is a powerful engine capable of efficiently performing complicated and large simulations, it relies on script input that must be painstakingly written and debugged by the user. Post processing is equally frustrating since there is no built-in way of visualising anything but the simplest results. To mitigate this issue, a general-purpose graphical user interface known as "GiD" was first extended by researchers for the standard version of OpenSees without thermomechanical capabilities [15,16], and then extended by the authors in the course of this work to incorporate their developments.

While OpenSees for fire has its own library of built-in fire scenarios, there is no way to automatically map temperature results from a CFD analysis to an OpenSees model for simulation of real fire scenarios, and the user must instead perform this manually one point at a time. Despite the tremendous development in both CFD and FEM modelling methods, the sequential coupling of both models is a challenging task mainly due to the difference in the spatial and temporal resolution of fire and structural domains. Over the last decades, considerable work has been done to couple FEM with CFD models [17–20]. While these computational tools can allow coupling between fire simulation, thermal and thermomechanical analysis their methods mainly target commercial software such as ANSYS and their codes are limited to small research groups of host institutions and are not open-source. This severely limits their usability by the research community and hinders the potential for collaborative

development.

This paper aims to fill this gap by linking fire simulation, thermal analysis, and thermomechanical via an open-source integrated simulation environment. This environment consists of three components: a 3D computer aided design (CAD) model containing information about geometry, an FDS model containing information about the fire, and a GiD model containing information about the HT and thermomechanical response and linking them with each other and with the FDS model. The first section of this paper discusses the individual components of the integrated simulation environment starting with FDS, HT, and then thermomechanical analysis and the extended GiD OpenSees interface. After this, the communication between these components and their integration into a unified environment is explained, and a programme built for faster HT analysis via parallel processing is introduced. Finally, a large demonstration example showcasing the efficiency with which the integrated environment enables simulation of tall and complex building structures is presented. It is hoped that with this work researchers and engineers from around the world will be able to tackle and study significantly more complex and notably larger simulation problems targeting tall and complex buildings in fire.

2. Numerical thermal and thermomechanical analysis of structures

2.1. Simulating fire with FDS

FDS is a powerful CFD software package for fire simulation that was developed by the National Institute of Standards and Technology (NIST) [21]. By solving the equations of conservation of energy, mass and momentum and associated chemical kinetics to model combustion reaction FDS is capable of realistically simulating the behaviour of fire and smoke [21]. This ability made FDS the simulation package of choice for studying the fires of the World Trade Center buildings 1, 2, and 7 [6,22,23], as well as the recommended fire simulation engine for the proposed integrated simulation environment presented in this paper.

2.1.1. Fire simulation sensitivity

Fire simulation deals mostly with turbulent flow which FDS solves using the large eddy simulation (LES) approach. In the LES approach, the energy and momentum are solved numerically only for eddies larger than the size of a single cell. For eddies that fall within the mesh size, energy and momentum are modelled approximately leading to FDS being very sensitive to the size of the mesh [24]. While there are a few theoretical methods to estimate a reasonable mesh size [25,26], for practical problems the authors recommend relying on numerical mesh sensitivity testing such as tracking the variation of gas temperatures for different mesh sizes.

In addition to the mesh size, parameters such as ventilation conditions, fuel location, chemical properties of combustibles, and even atmospheric conditions can result in the fire simulation deviating from the real modelled event [27]. Furthermore, even with tremendous development in modelling techniques over the last few decades, state-of-the-art fire models are still unable to simulate the gas-phase combustion reactions and complex pyrolysis and phase-change processes of solid fuels.

2.1.2. Thermal output

FDS can output temperatures, velocities in all dimensions, extinction coefficients, heat fluxes, and more. For HT analysis, the most relevant quantities are heat fluxes and temperatures that are applied as thermal boundary conditions. There are various methods to extract this data from the FDS simulation,

particularly: (1) Device output and (2) Plot3D (BNDF for solid phase devices). In the former, devices referred to from hereon as 'thermocouples', are installed at a point location where a quantity needs to be monitored over the course of the fire simulation. The output from the fire simulation provides a time history of the quantity in a comma-delimited file. Only the data required by the user at the thermocouples locations is recorded which reduces computational cost significantly. However, if after the simulation the user requires data at an unrecorded location then the entire simulation must be restarted. On the other hand, the Plot3D method will record the required gas parameter (temperature, velocity, etc) in binary form for each timestep and for each cell volume of the computational domain. This allows the user to access the results at any location after the simulation but comes at the cost of a higher computational demand and need for larger data storage. This can be a limiting factor for the models of tall buildings where the number of cells may be in the millions. The integrated simulation environment presented in this paper streamlines the creation of FDS thermocouples, and so the first approach is used where only the required FDS data is recorded. The gas temperatures obtained from the FDS simulation are translated via a python script into a time-temperature data format suitable for HT analysis in OpenSees.

2.2. OpenSees for thermal analysis

2.2.1. Heat transfer script and HT data

To facilitate heat transfer within the presented integrated simulation environment, a selection of predefined 2D heat transfer sections, shown in Fig. 1, were built into a parametric script that is run by OpenSees. The script receives a series of user-defined parameters defining the type of the section (composite beam, slab, regular I section, or stiffened I section), its dimensions, type of protection material and its thickness if any, and the properties of the fire and its duration. Each of the predefined sections was built up from rectangular 'block entities' which are then joined together using equal constraints between their boundaries. This constraint was also used between the blocks representing the concrete 'top flange' of composite beam sections and the top flange of the attached steel beam, as well as between the thermal protection and steel/concrete of the protected section. Temperature boundary conditions are applied around the perimeter of the I-sections, and to the underside of the slab and composite beam sections. The gas temperature boundary condition can be set to the standard fire, hydrocarbon fire, or user-defined fire. Ambient boundary conditions are applied at the top surface of the slabs and of the 'top flange' of the composite beam sections. Both convection and radiation are considered at these locations, with an average convective heat transfer coefficient for each of the fire and ambient boundary conditions defined by the user and used to calculate the heat flux from the gas temperatures predicted by FDS. By utilising gas temperatures instead of adiabatic surface temperatures or heat fluxes it is possible to refine the HT analysis by correcting for the value of the average convective coefficient for each member or for the analysis as a whole. In FDS, while evaluating heat fluxes or adiabatic surface temperatures, the convective heat transfer coefficient may be poorly defined for the cell. The significantly small size of boundary layer compared to the cell size makes it very difficult to incorporate a proper calculation of the convective heat transfer coefficient or the geometrical nuances of the different structural elements. This makes the computational analysis a blackbox where the user has no control over the estimates of the convective heat transfer coefficient. Using only gas temperatures gives the analyst more control over the errors introduced into the analysis. Meshing is also predefined for all the sections and is set to a reasonable degree of refinement.

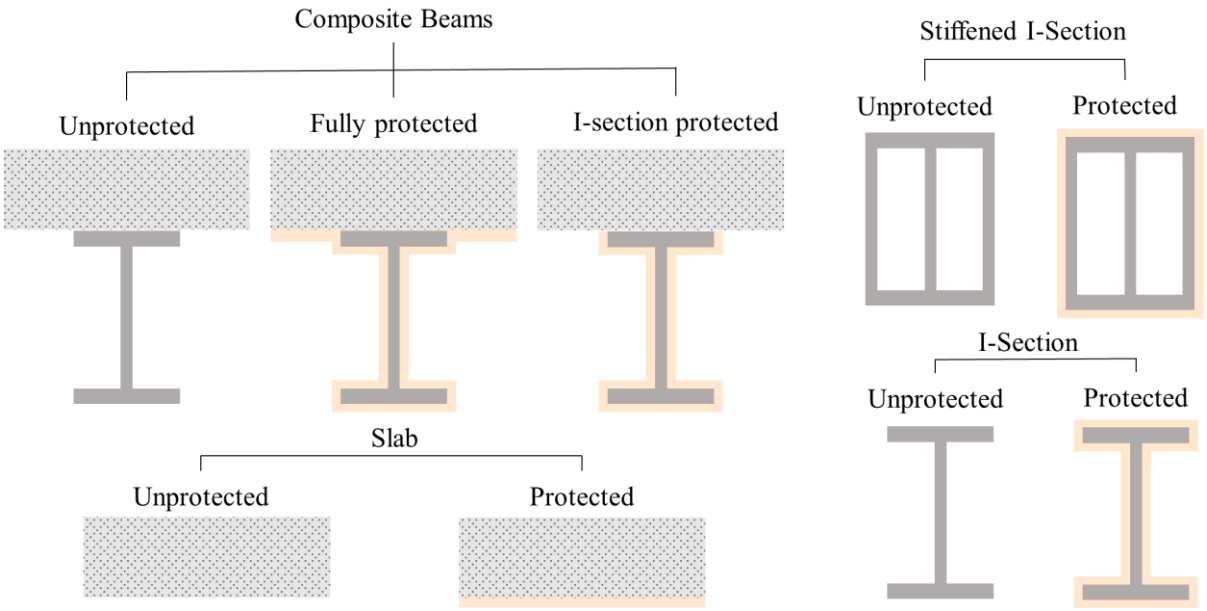

Fig. 1. Section types available for automatic heat transfer analysis

2.2.2. *Material properties*

The temperature-dependent properties of concrete and steel materials used in the OpenSees HT script follow the recommendations of the relevant Eurocodes such as the EN1993 for steel properties and EN1992 for the properties of normal weight concrete [28,29]. Unlike concrete and steel, it is more difficult to establish temperature-dependent thermal properties for insulation materials. As explained in Kodur and Shakya (2013), commercially available insulation material properties are often proprietary, and their temperature-dependent parameters are seldom known. To address this issue, Kodur and Shakya [30] experimentally tested the thermal properties of three spray applied fire resistive materials (SFRM), two of which are commonly used in the industry and the last of which has been gaining popularity recently. All the tested SFRM variants (CAFCO-300, Carboline Type-5MD, and Tyfo WRAFP) were gypsum based, and exhibited significantly different thermal properties that are highly sensitive to temperature, particularly in the 200 °C – 700 °C temperature range. The most important thermal properties for heat transfer in OpenSees, namely thermal capacity and conductivity, were adopted from Kodur and Shakya (2013) and the implemented expressions pertaining to their elevated temperature properties are given in Table 1. Here it is important to highlight that the original expression developed by [30] for the CAFCO-300 thermal capacity suffered from discontinuity across its limits since it is based on empirical data. To facilitate computational analysis in OpenSees, these minor discontinuities were marginally smoothed, and the thermal capacity relationship implemented in OpenSees takes the modified form shown in Table 1. In addition to the thermal properties from Kodur and Shakya (2013), the material properties from Li et al. [31] for another variant of the Carboline SFRM are also adopted into OpenSees and are shown in the table. Unlike the temperature-dependent relationships for thermal capacity from [30], the relationship for the Carboline variant used in Choe et al. (2019) and Li et al. (2020) is assumed to not vary with temperature.

Table 1. Thermal properties used for different types of insulation material in OpenSees

	Thermal conductivity (W/mK)	Thermal capacity (J/kgK)
CAFCO-300	$k_t = \begin{cases} 0.0778 - 0.000054T & 20 \le T < 300 \\ -0.08 + 0.000469T & 300 \le T \le 700 \end{cases}$	$^* c_p = \begin{cases} 3236 + 5.295T & 20 \le T < 200 \\ 7089 - 13.97T & 200 \le T < 400 \\ 1645 - 0.36T & 400 \le T < 700 \\ 1393 & 700 \le T < 1200 \end{cases}$
Carboline Type-5MD	$k_t = \begin{cases} 0.121 - 0.000319T & 20 \le T < 200 \\ 0.0468 + 0.00005T & 200 \le T \le 700 \end{cases}$	$c_p = \begin{cases} 1627 + 22.3T & 20 \le T < 100 \\ 4446 - 5.05T & 100 \le T < 400 \\ -1336 + 9.37T & 400 \le T \le 700 \end{cases}$
Tyfo WR-AFP	$k_t = \begin{cases} 0.207 - 0.000318T & 20 \le T < 200 \\ 0.147 - 0.000035T & 200 \le T < 400 \\ 0.0054 + 0.000321T & 400 \le T \le 700 \end{cases}$	$c_p = \begin{cases} 643 + 1.93T & 20 \le T < 200 \\ 1241 - 0.924T & 200 \le T < 400 \\ 195 + 1.71T & 400 \le T < 600 \\ 1826 - 1.08T & 600 \le T \le 700 \end{cases}$
Carboline, [31]	$k_t = \begin{cases} 0.11 - 0.00028T & 20 \le T < 750 \\ 0.32 & 750 \le T \le 1200 \end{cases}$	$c_p = 1111$

*modified expression for continuity

2.2.3. *Validation of HT parametric script*

One of the protected composite beams tested by Choe et al. (2019) and studied by Li et al. (2020) was modelled using the parametric heat transfer script and was run using OpenSees. The beam was a typical W18×35 wide flange beam protected with 19 mm of the Carboline variant from Li et al. (2020), and an unprotected light weight concrete slab 83 mm deep. A convective heat transfer coefficient of 25 W/m^{2}K was used with the experimental temperature-time curve for a 100-minutes HT analysis running with a time step of 5 seconds. Unfortunately, there is currently no functional material model for lightweight concrete available in OpenSees, and so the properties of normal weight concrete were used for the concrete 'top flange' of the composite beam. The Eurocode lumped temperature iterative method [29,33] was also used to predict the temperature of the steel section to provide a baseline prediction for comparison with the results of the HT analysis model. The lumped temperature method was performed using a weighted mean value for conductivity that did not change with temperature and ignored the heat capacity of the SFRM. The same timestep of 5 seconds was used for this analysis. The simulation results from the OpenSees HT analysis as well as the predictions of the numerical simulation performed by Li et al. (2020) and the experimental results are compared for the web and top flange of the steel section in Fig. 2 (a) and (b) respectively. For the web, which was heated from both sides and is the thinnest part of the steel section, the results of the numerical simulations and lumped temperature predictions are in very good agreement. Likewise, the numerical predictions by OpenSees and from Li et al. (2020) are very close for the top flange. This indicates that the current computationally inexpensive 2D OpenSees script is producing predictions that are of a similar quality to a significantly more sophisticated 3D numerical simulation. However, both the OpenSees and the Li et al. (2020) numerical results overestimate the temperatures reached in the steel beam by about 140 °C for the web and about 160 °C for the top flange.

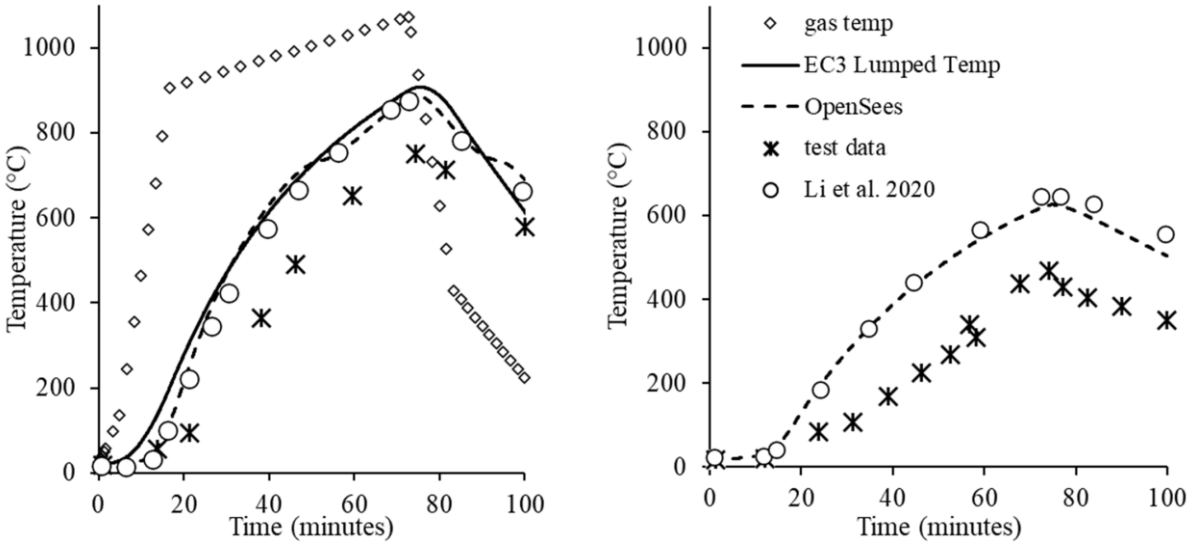

Fig. 2. Heat transfer results and comparison with results from [31] for (a) web and (b) top flange

2.3. OpenSees for thermomechanical analysis and GiD

OpenSees has undergone significant enhancements over the last decade to perform thermomechanical analysis. Amongst these, the most recent has been the inclusion of concrete damage plasticity material (CDP) and nonlinear shell elements for modelling floor slabs [34]. These two developments have been shown to compare well with analytical solutions, as well as with experimental data and numerical models developed by other researchers as shown in Fig. 3. Thermomechanical displacement-based and force-based beam-column elements as well as fibre-based force-deformation cross are also available with a library of thermomechanical material [13,35]. Thermal load can be applied to the shell elements at up to nine temperature points across the depth, and up to 15 points across the cross section of a fibre-based beam-column cross section.

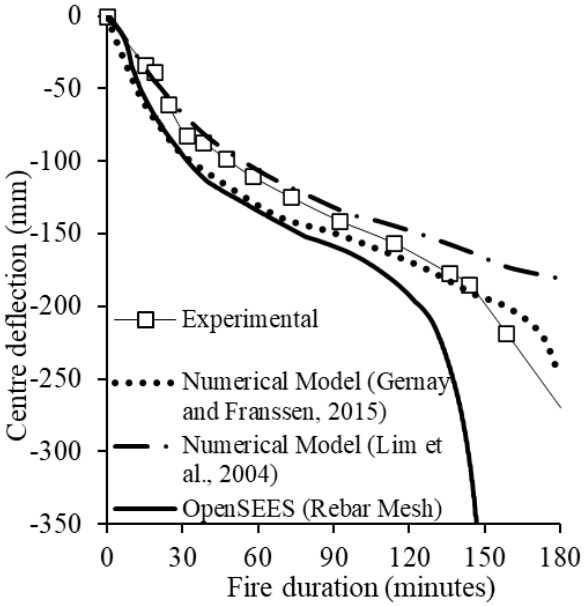

Fig. 1. Validation of OpenSees CDP material and shell elements. Reproduced from [34]

One of the major drawbacks to the thermomechanical capabilities of OpenSees is the difficulty involved in model building. As a researcher-developed open-source computational framework,

OpenSees relies on script-based input where the user has to manually define the nodes, materials, elements, constraints, and loads. Despite this, researchers have previously used OpenSees to build large models and analyse complicated load cases. The process usually relies on full simulation in other software and then like-to-like translation into OpenSees code [36,37], or laborious construction of large scripts using common programming tools [34]. Neither of these approaches is practical, and in the case of the latter there remains many difficulties in visualising large-scale results.

GiD is a general purpose pre and post processor equipped with a modifiable codebase and a graphical user [16]. It has been used by researchers from the Aristotle University of Thessaloniki to develop an open-source graphical user pre and post processor interface for OpenSees [15]. This interface has then been extended by the authors to incorporate thermomechanical sections as shown in Fig. 4 (a), material, elements, and prescribed thermal load as in Fig. 4 (c). More importantly, the GiD OpenSees interface serves as the centralised hub for the integrated simulation environment where creation of thermocouples, generation of HT data, performing the HT analyses, and creation of the OpenSees thermomechanical script file can be performed from the interface menu Fig. 4 (d). The 'Thermocouples' window seen in Fig. 4 (b) allows the user to apply a new kind of thermal load over beams, columns, slabs, and composite sections. Instead of prescribing a direct thermal load or field as is the classical approach, GiD assigns an identification number to each user-defined thermocouple and then uses that information to apply the correct temperature files to the right entities after mesh generation. The thermocouples are assigned to geometrical surfaces and lines, allowing the analyst to have control over their number and location by choosing the divisions of the GiD geometric entities before meshing.

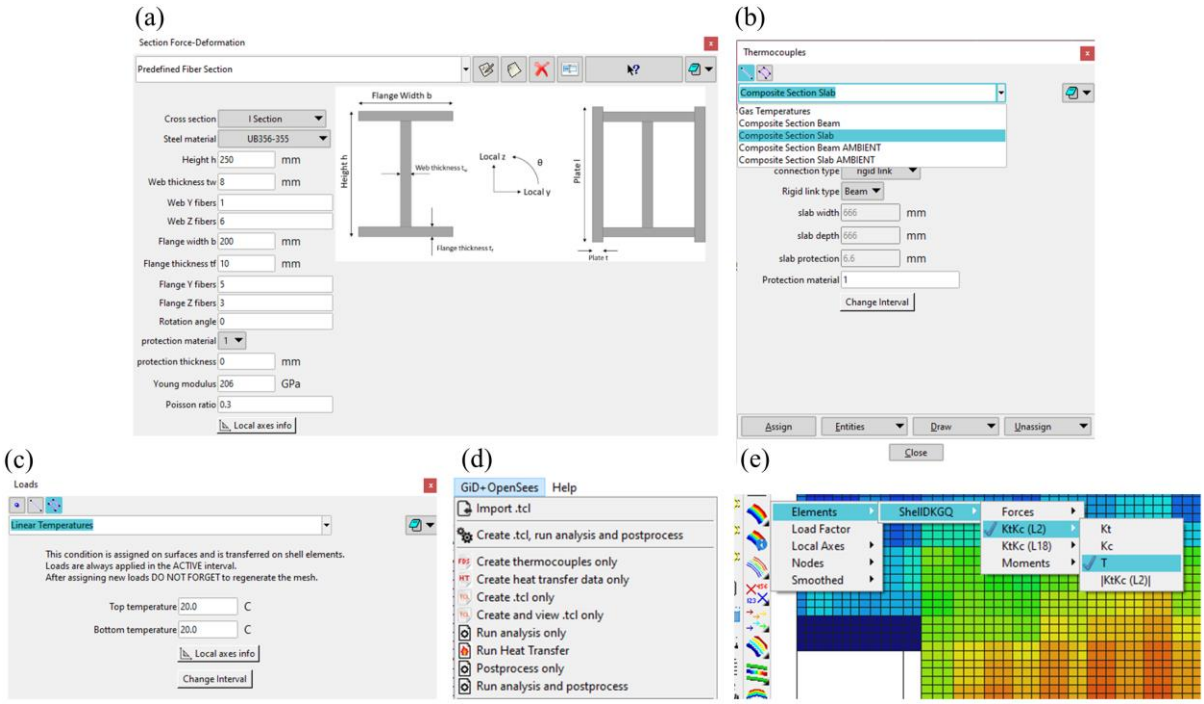

Fig. 4. The extended GiD + OpenSees interface (a) thermomechanical fibre section definition interface, (b) definition of thermocouples and composite section connectivity, (c) assignment of direct thermal load, (d) menu for navigating the steps of the integrated simulation environment, and (c) post processing interface

The conditions “Composite Section Beam” and “Composite Section Slab” are also available from the thermocouple window shown in Fig. 4 (b), and both can be applied to GiD geometric line entities according to Fig. 5 (a). The first condition is applied to the steel beam of a composite section, while the second is applied to the line dividing the geometric surface entities on either side of the composite beam section. The surfaces divided by the line assigned the “Composite Section Slab” condition will become the concrete ‘top flange’ of the composite beam. After the mesh is generated, which is illustrated in Fig. 5 (b), the nodes of the shell elements above the nodes of the beam-column element will be constrained to them using rigid links, equal degree of freedom constraints, or the two node sets will be merged achieving full transfer of translations and rotations. The method of connectivity is chosen by the user, but the linking is performed automatically by the interface. Each set of two surfaces and one line joined in this way constitute a composite beam unit, and the thermal load applied to them will depend on the HT results of a composite section type entity as shown in Fig. 1. Finally, Fig. 4 (e) demonstrates how GiD OpenSees has also been extended with additional functionality to display thermomechanical analysis results such as temperatures and concrete damage.

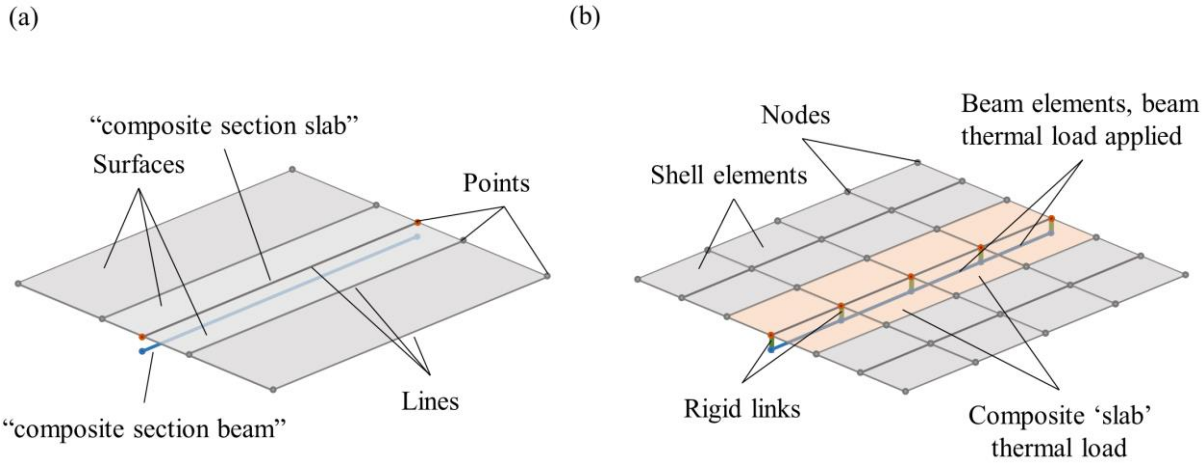

Fig. 5. ‘Smart’ composite beam connectivity and thermal loading (a) applying “composite section” conditions over the geometry, and (b) automatic connectivity and thermal loading over the mesh

3. Integrated simulation environment

The integrated simulation environment is a collection of all the aforementioned developments centred around the GiD OpenSees interface and made to interact in an organised workflow to efficiently develop sophisticated models for large and complex structures in fire. This environment is made to be simple and adaptable to the workflow of multi-disciplinary engineering teams that aim to tackle complicated structural fire problems.

3.1. Workflow and component interfacing

In modern design practices for tall or complex structures, it is expected that a 3D CAD building model is one of the design deliverables and would not need to be particularly made for the structural fire analysis. By starting the workflow from a CAD model, it becomes relatively efficient to integrate the structural fire analysis into the overarching design workflow. As shown in Fig. 6, given a CAD (in this case a Revit) model it is straightforward to export the geometry and build both a GiD model and an

FDS model. The model building process including assigning the sections, materials, and simulation variables can proceed in parallel in collaboration between the fire and structural engineers. Before the fire analysis is performed on FDS, thermocouples must be assigned within GiD by first selecting the thermocouple locations and then running the GiD mesh engine which will assign an identification number to each thermocouple before mesh generation. After the meshing is complete, these identifiers are propagated to the mesh elements. Exporting the thermocouples defined in GiD to FDS is the next step, and this is directly performable from the GiD menu in Fig. 4 (d). The format of the exported thermocouple file has been set to be that of the FDS file format so that it can simply be copied directly into the FDS script. By automating the creation of the thermocouples, the information transfer becomes a one-way process from the GiD model (structural engineer) into the FDS model (fire engineer). This eliminates the need for manual mapping of thermocouples between the two computational domains (structural and fire) and would reduce the amount of replicated work on both models as only one set of data definition needs to be made. This makes the current approach significantly less prone to error and more time efficient thus allowing for assessment of spatial refinement of thermal data that would not be feasible within a manual workflow.

The fire simulation may begin immediately after the thermocouples file is generated and imported into the FDS model. To perform HT analysis, the information of each section at which a thermocouple was assigned must be aggregated into a unified data file. This data file is generated into the working directory of the GiD model directly from within the GiD interface and will collect the section information automatically from every element that is assigned a thermocouple without the need for any additional user input. Once the FDS fire simulation is completed, the gas temperatures are translated via the Python translation script discussed in *section 2.1.2* into OpenSees-compatible boundary condition files containing gas temperatures. Each of the FDS gas temperature files corresponds to the location of a single thermocouple and will have associated with it a single line in the HT data file. To run the heat transfer analysis the user then manually copies the FDS-generated temperature files into the directory of the GiD model and calls the heat transfer process from the GiD OpenSees interface. Considering that each of the heat transfer analysis constitutes the solution of a full FEM problem for thousands of timesteps, a parallel programme was written to cut down on the total computational time required by distributing the workload over multiple processors. This is particularly useful for larger models containing thousands of thermocouples, and hence requiring thousands of HT analyses. Details of the parallel programme are discussed in the next section.

The HT analyses result files are placed in a sub directory within the GiD project working directory. Depending on section type, each HT analysis result output consists of a thermal load file containing either 15 points for beam-column elements, or 9 points for shell elements. HT analyses performed for a composite section generates both a shell and a beam-column element thermal load files. The HT result files are associated with the mesh elements via the identification number assigned to the thermocouples before meshing and propagated unto the mesh elements after mesh generation. Finally, an OpenSees script containing all sections and both ambient and thermal loading is generated and run from within GiD, with the output results then compiled into a GiD database allowing for a level of post processing that was not feasible before in OpenSees for fire.

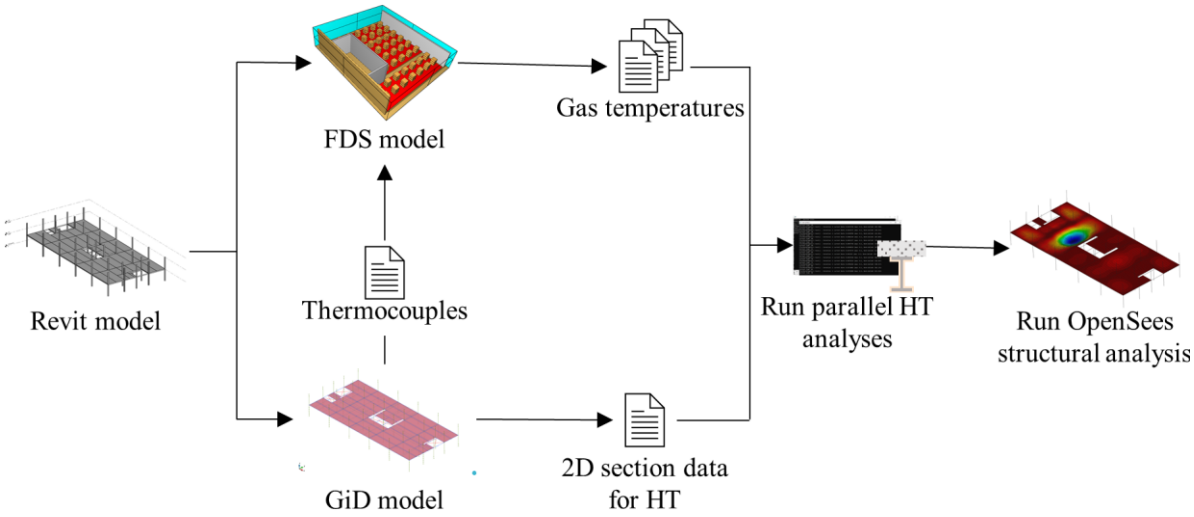

Fig. 6. Workflow for the integrated simulation environment incorporating fire simulation, heat transfer, and structural analysis

3.2. *Parallel heat transfer analyses*

Substituting a series of 2D HT analyses for 3D HT analyses to map gas phase temperatures from FDS to solid phase temperatures in the structural elements reduces the computational load considerably while maintaining a good level of accuracy [38]. In large or complex models, the number of required thermocouples and corresponding HT analyses can number in the thousands which then once again increases the computational cost. As the intermediary step between fire simulation and thermomechanical simulation, HT analysis should be performed more efficiently but without sacrificing accuracy. The HT script presented earlier sought to optimise the HT mesh and make sure that each HT problem solved is relatively inexpensive. Since each individual problem is inexpensive, it is possible to perform multiples of these problems simultaneously on the same machine. Modern processors including those in portable devices such as phones and tablets are now routinely equipped with multiple computing cores that enable efficient multiprocessing. This fact can be exploited by assigning each processor a unique HT problem to solve thus performing multiple HT analyses at the same time and reducing the overall analysis time.

To do this, a programme based on the manager-worker paradigm for multiprocessing was written in C++ with the MS-MPI library. This programme is included as part of the GiD OpenSees interface and is assigned to perform HT over four processors by default. The programme handles multi-processing by passing messages containing instruction sets between processors. Fig. 7 (a) through (d) explain how the programme works:

(a) When HT is called from within the GiD OpenSees interface, a processor designated with an ID of 0 is set as the ‘manager’, and is given the GiD-generated HT data file. The manager parses this file and separates it into a list of individual commands each of which constitutes the data for a single HT analysis.

(b) The manager sends a single command to each processor dedicated to the HT task except itself. Each of these processors, which are known as the ‘workers’, starts an instance of OpenSees and executes the HT problem that was assigned to it.

(c) When any of the processors completes the HT analysis it was assigned it notifies the manager

that is now free and available to perform another task. The manager in response assigns that worker another HT problem to solve. The results of the completed analysis are saved within the GiD project directory, and a log file is also generated containing information about the success or failure of the analysis.

(d) Upon completion of all HT tasks, the manager 'retires' the workers and then proceeds to inspect all generated log files. Based on the information in the log files, the manager writes a report file containing the identification number of each HT transfer problem and whether this problem was analysed successfully or not. If the problem failed to be analysed the manager indicates in the report file whether this failure occurred due to divergence of the numerical solution procedure or because of other issues such as incorrect data passed to the HT script.

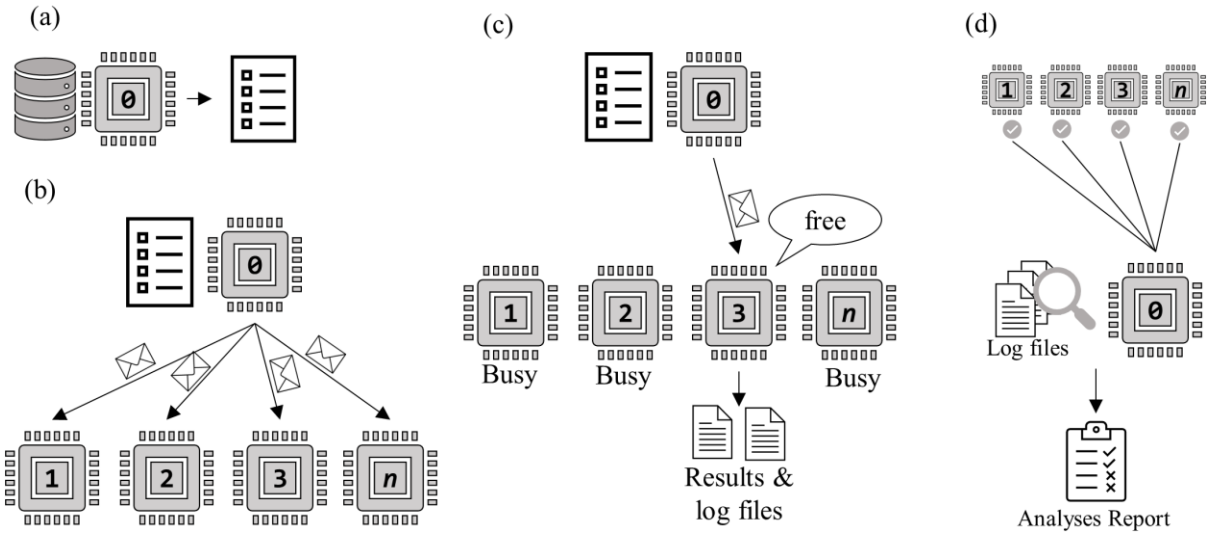

Fig. 7. Manager-worker paradigm for heat transfer (a) manager breaks problem database into individual command lines, (b) manager distributes work to workers, (c) once a worker completes a task and produces an output it asks for a new job from the manager, and (d) once all jobs are done workers are retired and manager checks log files and generates status report for the analyses

4. Cardington Large Compartment Test

The Cardington large compartment test was the largest test performed during the Cardington series of tests, and it involved over 340 m^2 of the floor area of a single floor. This experiment was chosen as a demonstration case for the current work. This is because (a) it represents a realistic form of construction used for tall and composite buildings, and (b) it is a large-scale test thus posing significant practical constraints to the classical simulation workflow. The goal of this demonstration is to showcase the efficiency of the presented simulation environment in handling large models, not to investigate the real behaviour of the Cardington large compartment test as that has been done by researchers in the past [39,40]. The first step towards this goal is to create a 3D Revit or other CAD model, such as the one presented in Fig. 8 (a), which has the dimensions and gridlines shown in Fig. 8 (b). A fire based on the general conditions of the experiment is then generated using FDS, accompanied by generation of a GiD model. HT based on the FDS results is then performed, and the structure is analysed and results are finally discussed.

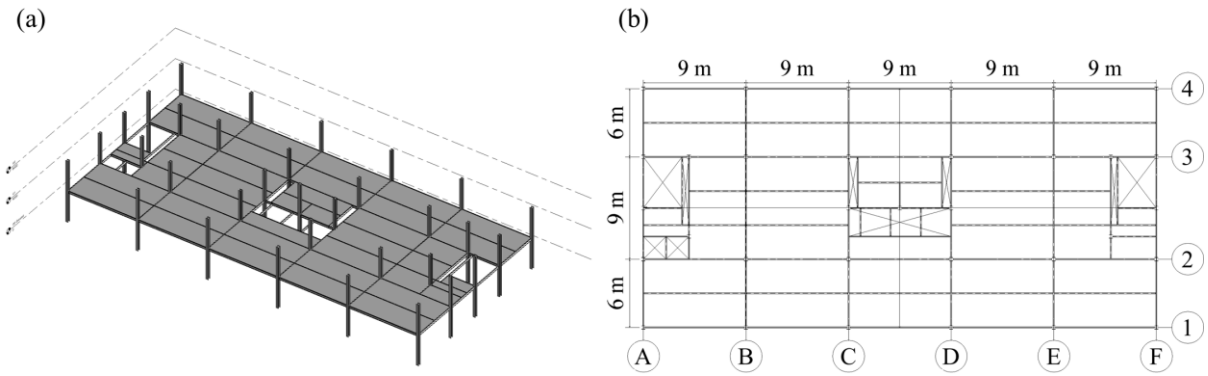

Fig. 8. Revit model for the Cardington building (a) 3D view, and (b) plan view

4.1. *FDS Simulation*

As per the integrated simulation workflow, an FDS model of the compartment used in the Cardington large enclosure test was created using geometrical information exported from the Revit model. Both north and south faces were assumed to be completely open and would allow for unhindered air flow. Fig. 9 (a) shows the compartment geometry and Fig. 9 (b) the computational domain. Wood cribs were used to fuel the fire of the test, and despite their practicality and widespread use for experiments, modelling their combustion remains an involved task. It has been shown that due to the complex chemical kinetics involved and scale of individual timber pieces used high-fidelity simulation of burning cribs may require a mesh size in the order of at most 0.05 m [21]. In this study, the cribs were simplified and abstracted as a collection of three 1 m × 1 m × 0.4 m blocks in FDS allowing for utilisation of a coarser mesh resolution that detailed simulation of the cribs would prohibit. To allow for the effect of porosity which would increase the burning rate due to the free movement of air [41] a 0.2 m gap was set between the blocks of each crib set as shown in Fig. 9 (a). The properties of wood were taken from the SFPE handbook and data available in the literature [41,42]. Mesh sizes of 0.3 m, 0.2 m, and 0.15 m were tested. The variation of gas temperatures between the three meshes indicated that a cell size of 0.2 m was suitable for the FDS analysis. The blocks were spaced at 1.5 m intervals and simulated a fuel load of 48 kg/m^2 (calculated as fuel per floor area), which is more than the fuel load of 40 kg/m^2 used in the actual test. As mentioned earlier, this FDS simulation was not intended to explicitly simulate the real test fire using this model but produce realistic spatially and temporally varying gas temperatures to demonstrate the ability of this framework to utilise complex, CFD-based heating fields for thermo-mechanical analysis of complex structures. An ignition temperature of 320 °C was assigned to the fuel, all of which was ignited using burners set for two minutes at the beginning of the analysis. The *burn-away* method was used to represent decay phase where once the mass of fuel in a cell volume is burnt out, the entire fuel volume would be deleted from the computational domain [21].

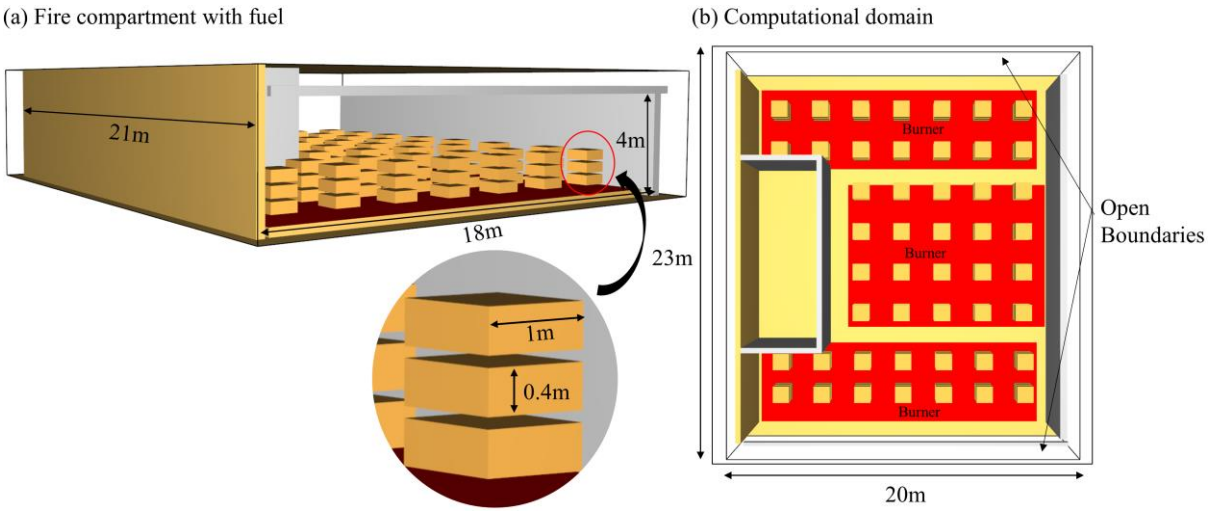

Fig. 9. Fire compartment and computational domain

Fig. 10 shows the fire simulation at three different time intervals. After the initial ignition event, which lasted for two minutes, the burner was turned off and all the fuel in the compartment had ignited as seen five minutes into the simulation in Fig. 10 (a). 45 minutes into the simulation, some of the fuel blocks already burnt out and were removed from the computational domain as per the burn-away method, as seen in Fig. 10 (b). Fig. 10 (c) shows the state of the simulation after two hours when all the fuel in the compartment was burnt out and only smoke remained within the compartment. The gas temperature contours for 3 m above the compartment floor for time stamps of 15 minutes, 60 minutes, and 120 minutes are plotted in Fig. 11. The highest temperatures are reached within the middle of the fire compartment, while the temperatures near the openings are significantly lower. This variation can be explained by the volume of cool air entering the fire compartment from the openings and mixing with the hot gases thus reducing the overall gas temperatures in the regions closest to the ventilation.

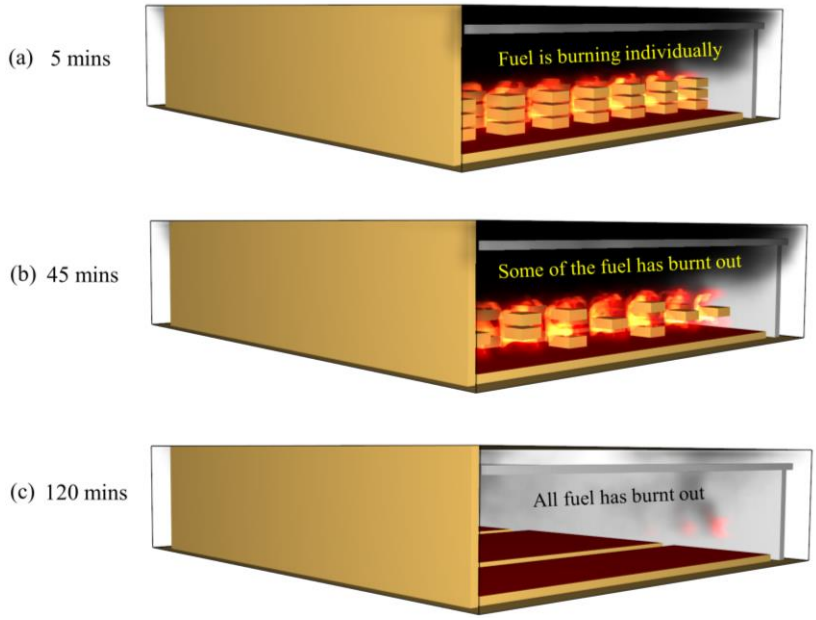

Fig. 10. Fire simulation (a) all fuel in the compartment is burning (b) some of the fuel is burned out (c) fuel fully consumed

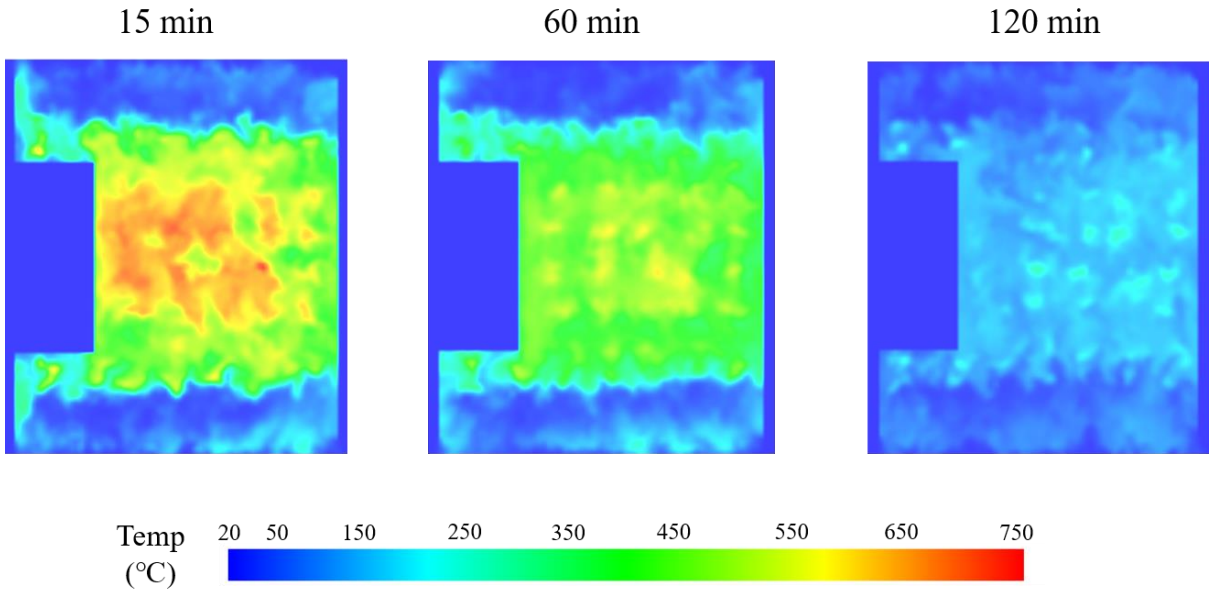

Fig. 11. Temperature contours at a height of 3 m from the floor

4.2. Thermocouples, Connectivity, and meshing

The floor of the Cardington building consisted of a 130 mm thick ribbed slab with 6 mm diameter 200 mm × 200 mm wire mesh. The ribs were 55 mm deep, and the steel decking had a thickness of 0.9 mm. Full connectivity between the slab and the floor framing was ensured using shear studs with a diameter of 19 mm. To represent the orthotropic effect of the ribs, researchers have used purpose-built finite elements [43,44], combination of beam and shell elements to represent the ribs and continuous portions respectively [34], and simplifications where the ribbed portion of the floor is ignored [7]. While the first approach may be the most sophisticated, its outcome is highly dependent on the quality of implementation employed, and its non-standard formulation means that it may not be widely available. OpenSees for fire does not yet have a working and validated ribbed section representation, although this is currently being developed. The second approach using beam elements to represent the ribs is feasible in OpenSees and has been used for structural fire simulation before [34]. The main issue with this approach is that it introduces a very large number of constraint conditions to link the nodes of the ribs and continuous segments of the slab together. While this may be tolerable in smaller models, the added computational expense may easily outweigh the benefit of potential added accuracy in larger models. Finally, by ignoring the effect of the ribs altogether one may get a far less expensive model that could possess a satisfactory level of accuracy depending on the purpose of the model. The intention of the presented simulation environment is to make more representative analyses feasible, and so ignoring the effect of the ribs is undesirable. To overcome these difficulties, a different approach is employed for the demonstration case where groups of ribs are aggregated together and then represented using shell elements.

Two-layered shell sections were defined for this purpose, a 130 mm section to represent the ribs, and a thinner 70 mm representing the continuous portion of the slab. These sections were alternatingly applied to the floor slab in the fire region as shown in Fig. 12. As will be shown later, representation of the thicker and thinner parts of the slab helps capture, although in a simplified fashion, the complex thermal state and thus thermomechanical response that is experienced by ribbed floor slabs.

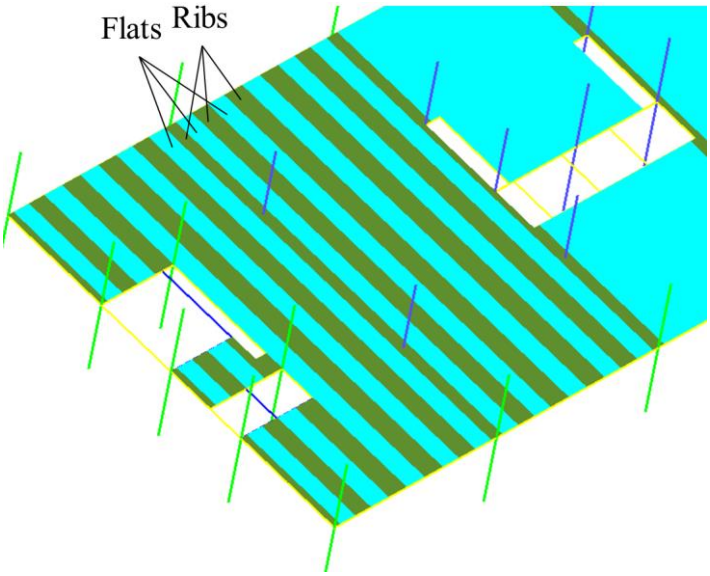

Fig. 12. Distribution of rib and flat sections for the slab

The distribution of the thermocouples within the floor is governed by the number of geometric divisions the user enforces over the model. For the demonstration case, slab thermocouples were distributed at intervals of approximately 1 m as shown in Fig. 13 (a). Likewise, the thermocouples for composite beams were spaced approximately 1 m apart, with the assumption that their temperatures and HT results apply over a 0.6 m wide 'top flange' area. As shown in the *section 2.3.*, the connectivity between the steel beams and their concrete 'top flanges' was established automatically at the nodal level by applying 'composite section beam' and 'composite section slab' conditions over their respective geometric lines. The floor slab shell elements were offset by 70 mm from the beam elements, and 'beam' rigid links that transfer both rotations and translations were chosen here to represent the full composite action and incorporate the dowel action caused by differential heating. The mesh used was relatively fine with element length set to 0.3 m, resulting in at least nine elements representing each slab thermocouple, and six elements representing each composite beam 'top flange' at each thermocouple location as shown in Fig. 13 (b). The fine mesh used here was chosen to allow the distribution of concrete damage to spread in a more natural manner reducing the mesh-dependency reported for distributed cracking methods [45]. As per the workflow of the integrated simulation environment, at each thermocouple location an appropriate HT analysis was performed, and the results were then automatically applied to the correct mesh elements. In total, there were 996 thermocouples and over 11,000 nodes, 7,200 shell elements, and 3,600 beam-column elements. Performing the thermomechanical analysis in OpenSees solver took just under 4 hours on a regular i7 3.00 GHz desktop computer.

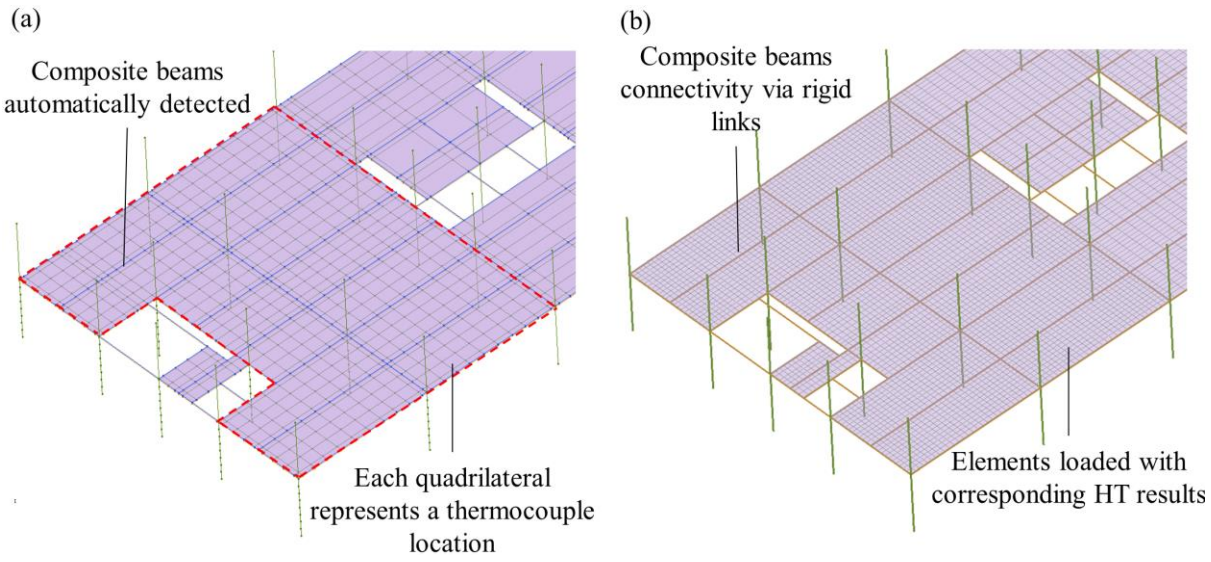

Fig. 13. GiD model (a) geometry and thermocouples distribution, and (b) mesh

4.3. Heat transfer results

Representing the ribbed slab using two types of shell element sections allowed the effects of spatial variation of temperature and the heat-sink effect of composite beam 'top flanges' to be clear after the HT analysis. Fig. 14 (a) presents the evolution of temperature in the bottom layer of the layered slab sections over 90 minutes of the fire. As discussed in *section 4.1.*, the hottest gas temperatures were located within the middle of the fire compartment within the region enclosed by gridlines B, C, 2, and 3 (Fig. 8). The perimeter of the building outside gridlines 2 and 3 stayed relatively cool throughout the analysis. The hottest temperatures within the floor slab were achieved after about 1 hour of heating, with the thinner portions of the slab reaching higher temperatures faster due to their lower thermal mass. Moreover, the presence of composite sections resulted in the initial emergence of cooler zones along the length of the beams, such as that seen 15 minutes into the fire over the largest floor beam along gridline B and within gridlines 2 and 3. This phenomenon is reversed during cooling, which takes place after 60 minutes as per Fig. 14 (a) which showcases the FDS gas temperature against time for the middle of the compartment. At 75 minutes it is observed from Fig. 14 (a) that the shell elements atop the composite beams remain hotter than the adjacent slab. The composite steel beams below these segments initially acted as thermal barriers and heat sinks protecting the slab from direct convection and radiation during heating. During cooling, the energy that the steel beams absorbed was slowly released into the atmosphere while preventing the slab from cooling rapidly. This effect can still be seen even 90 minutes into the fire and 30 minutes after the highest temperatures were reached. The top surface of the slab experiences a different thermal history. As shown in Fig. 14 (b), the thick and thin layered sections produce a clear effect with the thin sections reaching maximum temperatures of about twice the thicker sections. As expected, the top surface temperatures continued to increase for over 30 minutes after the peak gas temperature was reached.

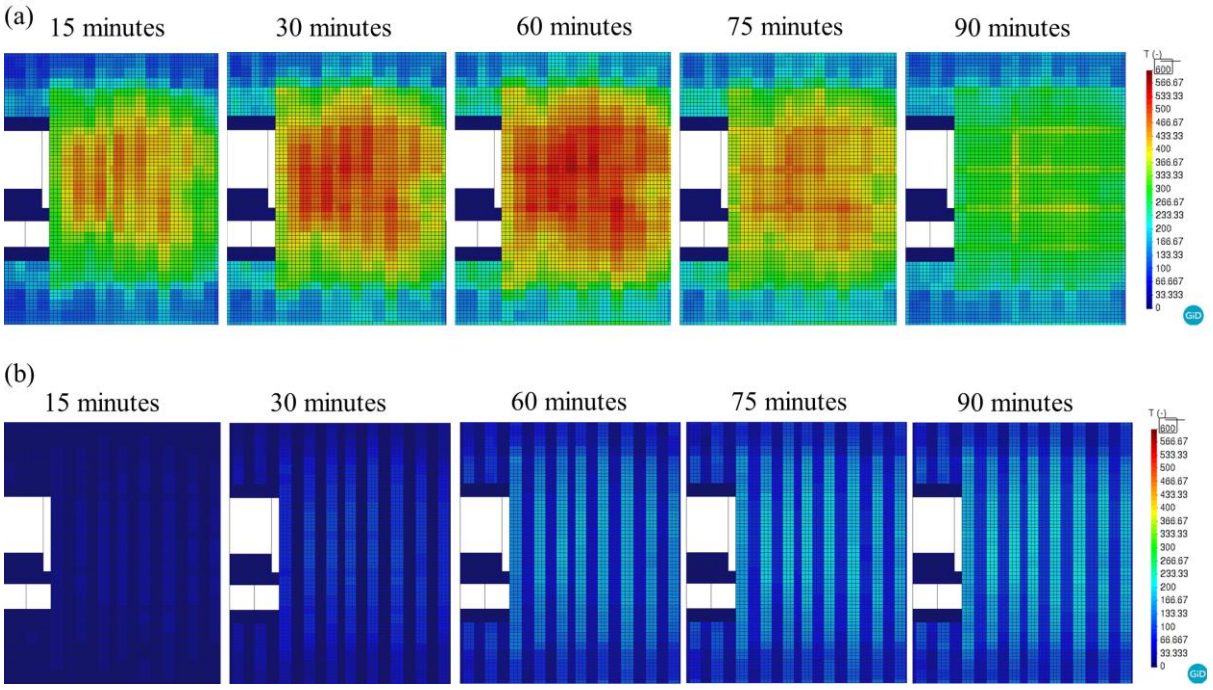

Fig. 14. Temperature growth (a) in the bottom layer of the slab, and (b) in the top layer of the slab

It is noted in Moss and Clifton (2004) that the temperature within the fire compartment was generally uniform and could be averaged as shown in the temperature-time curve in Fig. 15 (a), which is contrary to the FDS results used in this demonstration which showed stark spatial variation. Two abnormalities presented in the FDS gas temperature-time curve: an initial momentary spike in temperature reaching 800 °C, and a 'stepwise decrease in temperature after uniform 600 °C temperatures for 60 minutes. The first occurred, as explained in *section 4.1.*, due to the artificial ignition of all cribs at the same time using burners for the first 2 minutes of the analysis. The second phenomenon is an artifact of the prescribed combustion behaviour of the wooden cribs and their abstraction as simple blocks. Because of these reasons, the gas temperatures from the current FDS analysis appear less 'natural' than the average experimental temperature-time curve. However, these spatially varied temperatures present by far the more interesting case for both the kind of academic study presented here and for practical application where the conditions for uniform temperatures across a large compartment are unlikely to be met.

Fig. 15 (b) shows the thermal gradient achieved by a composite beam located within the middle of the fire compartment. Since none of the beams in the test were protected, the steel temperature in the bottom flange rises to the proximity of the gas temperature within minutes from ignition. The top flange, however, remains relatively cooler due to the heatsink effect of the slab. The bottom of the slab is tied to the top of the beam with an equal degree of freedom constraint during the HT analysis and thus is at the same temperature as the top flange. The temperature within the middle of the slab and at the top surface is also plotted demonstrating the nonlinear temperature profile within the concrete 'top flange' of the composite beam. While the temperature in the steel beam and bottom of the slab enters the cooling phase shortly after the peak gas temperatures are traversed, the concrete within the slab continues to heat up to around 90 minutes. It is crucial to note here that the consideration of the steel beam and concrete slab as a unified HT cross-section and as linked structural components enables the

development of large thermal gradients and for the effects of these gradients to be considered. It has been shown elsewhere [46] that a thermal gradient on its own is sufficient to trigger tensile-membrane action in thin slabs, and has been recognised as one of the key actions producing large deflections and inducing secondary forces in composite beams [47,48]. The thermal gradient within composite floor beams of large structures should always be considered, as is done in this demonstration and facilitated by the presented integrated simulation environment.

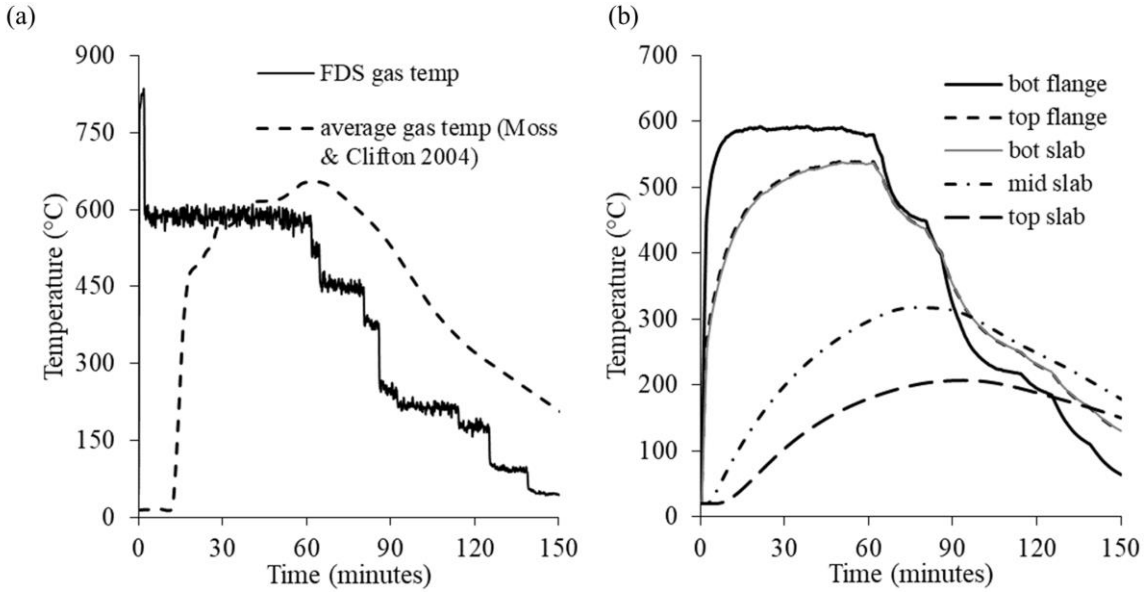

Fig. 15. Temperatures in the model (a) FDS gas temperatures in middle of the compartment and average compartment temperature from [39], and (b) thermal gradient achieved in a composite beam subject to FDS gas temperatures

4.4. Deflected shape and displacements

Upon studying the deflected shape in Fig. 16 it is evident that the unheated structure experiences only minor deformations, as expected. The largest deflections occurred in the middle of the fire compartment marked as 'Location 1' in Fig. 16. 'Location 2' was also instrumented, and results were available [39]. The deflection at these two locations is plotted in Fig. 14 (a) and (b) respectively. In addition to the test data and numerical predictions from the demonstration case, numerical predictions from Moss and Clifton (2004) are also shown. For completeness, the test temperature-time curve presented in Fig. 12 (a) was applied to the model using the integrated environment, and results from that analysis are also shown. The results from the demonstration case are vastly different from the experimental results. This difference is caused by the different heating regimens the test and demonstration case were subjected to, which becomes evident when the test temperatures were applied uniformly to the heated region. The deflection results very close to the test results at location 1. The application of uniform temperatures across the entire area also meant that location 2 was subjected to the highest temperatures just like location 1, which if the FDS results are taken as a general indicator of 'hot' and 'cool' zones was not the case. These high temperatures caused the composite beams in that region to exceed the experimental results significantly. The very cool temperatures generated by FDS at location 2 resulted in very small deflections at that location as predicted by the demonstration case.

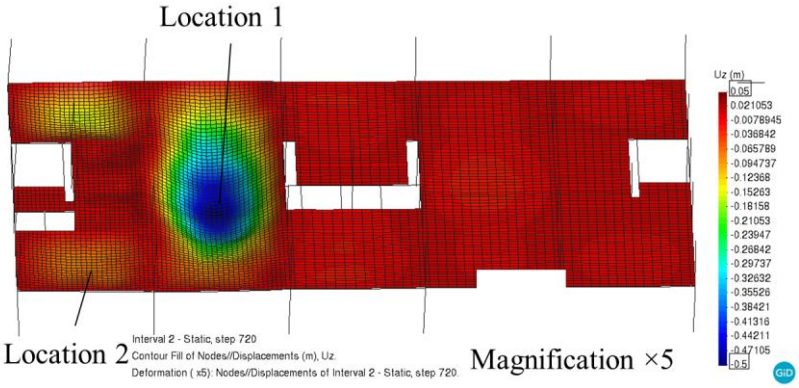

Fig. 16. Deflected shape of the model subject to FDS temperatures (×5 magnification factor)

The largest deflections occurred in the middle of the fire compartment marked as 'Location 1' in Fig. 16. 'Location 2' was also instrumented, and results were available for its deflection from Moss and Clifton (2004). The deflection at these two locations is plotted in Fig. 17 (a) and (b) respectively. In addition to the test data and numerical predictions from the demonstration case, numerical predictions from Moss and Clifton (2004) are also shown. For completeness, the test temperature-time curve presented in Fig. 15 was applied to the model using the integrated environment, and the results from that analysis are also shown. As expected, the results from the demonstration case are different from the experimental results with significantly steeper initial deflections caused by the abrupt heating. The different heating regimens the test and demonstration case were subjected to are shown to be responsible for the behaviour when the test temperatures were applied uniformly to the heated region resulting in more representative deflections of the test at location 1. The application of uniform temperatures across the entire area also meant that location 2 was subjected to high temperatures just like location 1, which if the FDS results are taken as a general indicator of 'hot' and 'cool' zones was not the case. These high temperatures caused the composite beams in that region to exceed the experimental results significantly. The cooler temperatures generated by FDS at location 2 produce a better prediction of the maximum deflection, which indicates that this area indeed experienced significantly cooler temperatures.

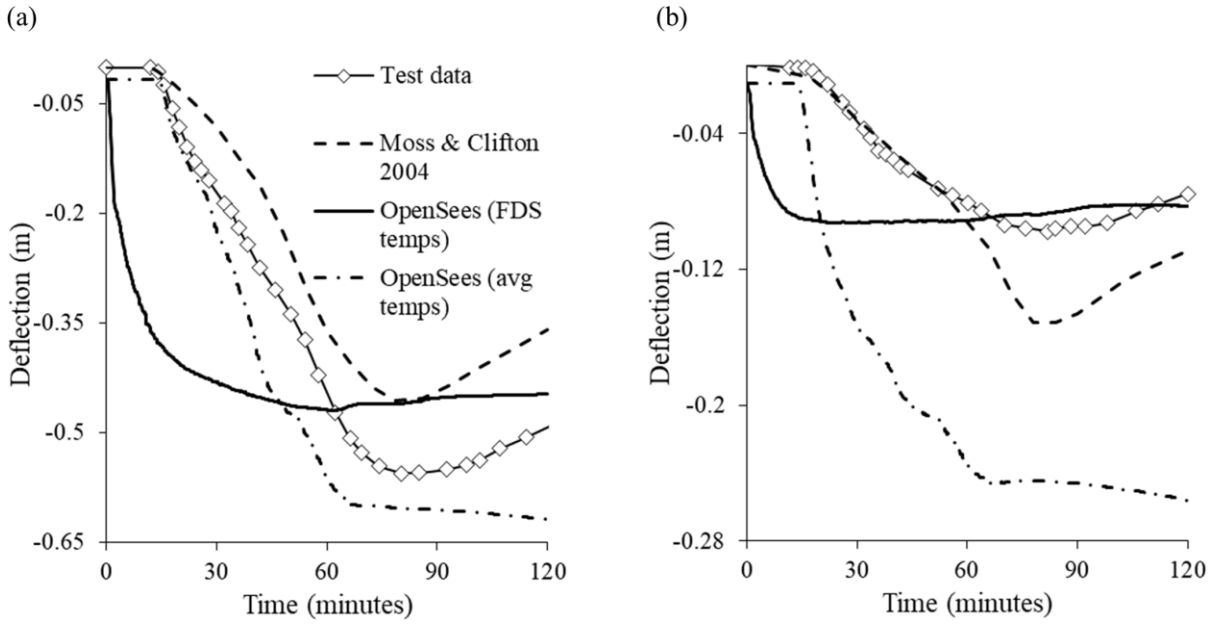

Fig. 17. Deflections from the experiment, numerical analysis by [39], and from OpenSees for (a) location 1, and (b) location 2

4.5. *Damage*

The concrete damage plasticity material model used for the shell elements in this simulation environment is governed by damage parameters that track the accumulation of compressive and tensile cracking and their recovery upon load reversal [34]. Therefore, by tracking the tensile damage variable at the top layer of the concrete, Fig. 18 can present a visualisation of the potential top layer cracking the structure may exhibit. Amongst the clearest indicators of damage observed in composite floors in fire is the early cracking of their perimeters at the locations of connection to large girders and columns [49–51]. This phenomenon seems to present as early as 1 minute into the thermomechanical analysis where the highest damage is first accumulated over the largest composite beam. From there, the damage begins to spread rapidly and from over the composite beams. By the end of the analysis, the top concrete layer is shown to have experienced significant cracking throughout the fire compartment, with damage spreading over to the unheated structure. This is the reason why the lack of high deflections in the compartments unexposed to fire should not be the only consideration for whether to include them in the analysis. These adjacent bays may play an important role in applying finite restraint to the structure and may experience interesting phenomenon such as extended cracking as shown here and even more clearly in the large-scale experiment presented in Yang et al. [52]. Nevertheless, caution must be advised when interpreting the damage parameter results as they can only give a general idea of the expected damage pattern at a particular layer. Tracking the coalescence, and propagation of through depth cracks, and even discrete surface cracks, requires more sophisticated approaches that employ the extended finite element method [45] or other advanced implementations and solvers.

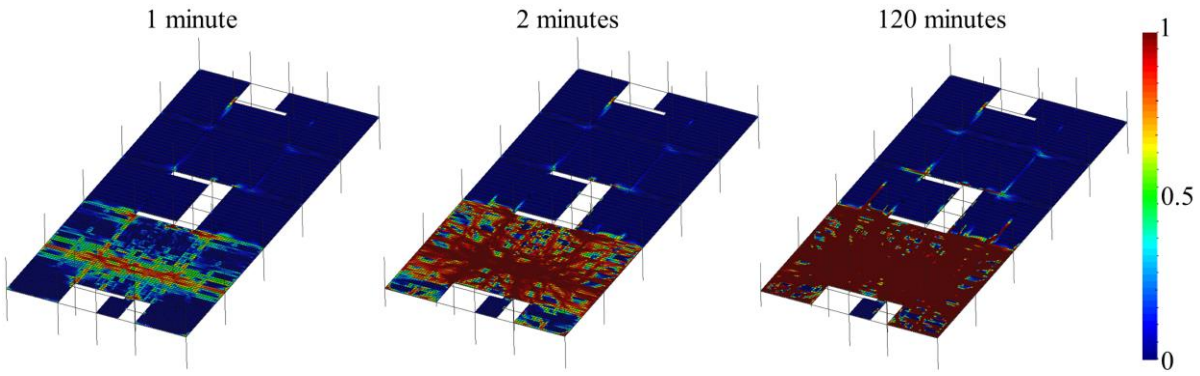

Fig. 18. top layer tensile damage parameter where 1 indicates full damage

5. Conclusions

This article discussed recent developments in the simulation of tall and complex buildings in fire, presented an open-source integrated simulation environment that allows for modelling them efficiently, and then used a demonstration study to showcase the abilities of the developed environment. The simulation environment links models built in CAD, fire simulation in FDS, as well as HT and thermomechanical analyses in OpenSees via the GiD OpenSees interface. The GiD OpenSees interface generates the FDS thermocouples and the data required for HT, performs HT transfer analysis over multiple processors, assigns the results to the mesh as a thermal load, and produces an OpenSees script for thermomechanical analysis. Finally, GiD combines the results into a database for post processing allowing OpenSees for fire results to be visualised in a way that was not possible before. The key conclusions from this work are:

(1) While FDS is capable of realistic fire simulation and was the tool of choice for some of the most complicated fire problems [6,22] in the field, it still has some shortcomings. Due to its use of the LES approach for capturing the effects of turbulence, FDS is highly sensitive to mesh size. Parameters such as ventilation, fuel distribution and properties, as well as atmospheric conditions all affect FDS simulation outcomes and thus should be considered very carefully. FDS is still recommended as the fire simulation software for this work because its strengths far outweigh its downsides which can be mitigated by sound and informed engineering judgement.

(2) The OpenSees HT script presented in this paper is capable of accurately assessing the temperatures within protected structural members as shown by validating against experimental and numerical results from Li et al. (2020). The thermal properties for SFRM implemented in OpenSees are based on the work by Kodur and Shakya (2013) and Li et al. (2020).

(3) The GiD OpenSees frame work from [15] was extended to incorporate thermomechanical materials, sections, elements, and loads. In addition, ‘thermocouples’ were implemented in GiD OpenSees to seamlessly create FDS devices and then use the results for heat transfer analysis in OpenSees. Composite section definition was also added to GiD OpenSees to automatically establish connectivity between the shell elements and beam-column elements representing the concrete ‘top flange’ and steel section of composite beams, respectively.

(4) The Cardington large compartment test was used a demonstration case for the integrated simulation workflow. A Revit model was built, and its geometric information imported into GiD and FDS. An FDS analysis was run and generated gas temperatures that were significantly

higher in the middle of the fire compartment than near the openings. These temperatures were monitored over 996 thermocouple locations and used for heat transfer analysis and then thermomechanical analysis. The maximum deflections achieved were within about 20% of the experimental deflections but followed a starkly different pattern. This was primarily caused by the difference between the FDS simulation and the real fire. Damage patterns tracked using the concrete damage parameters point towards cracking initiating from above the largest floor beam and extending over the composite beams due to the restraint. Damage enveloped the entire compartment by the end of the test and even extended into the unheated portions of the floor.

(5) Performing a simulation of the scale and level of details as the demonstration example would be a hugely cumbersome task if not for the integrated simulation environment handling the mapping of thermocouples, generation of HT data, and performing of HT and then assigning the results and connectivity to the mesh. Within this environment it is now possible for researchers and engineers to tackle much larger problems more effectively and efficiently while making better use of the computational power that is now routinely available at their disposal.

(6) All the developments mentioned in this work are open-source, and interested readers are encouraged to test these tools for themselves. The required software is available on GitHub and can be found by contacting the corresponding authors.

Acknowledgements

This research is funded by the RGC Hong Kong GRF Scheme (No. 15220618) and SLDRCE Open Fund (SLDRCE20-02) from the State Key Laboratory of Disaster Reduction in Civil Engineering.

References

[1] J.L. Torero, Grenfell Tower, Expert Report, 2018.

[2] L. Bisby, Grenfell Tower Inquiry, Expert Report, 2018.

[3] A.A. Khan, S. Lin, X. Huang, A. Usmani, Facade Fire Hazards of Bench-Scale Aluminum Composite Panel with Flame-Retardant Core, Fire Technol. (2021). https://doi.org/10.1007/s10694-020-01089-4.

[4] A.A. Khan, A.S. Usmani, J.L. Torero, Evolution of fire models for estimating structural fire-resistance., Fire Saf. J. (2021). https://doi.org/10.1016/j.firesaf.2021.103367.

[5] CEN, Eurocode 1 : Actions on structures BS EN 1991 -1-4, 3 (2005) 152.

[6] NIST, NIST NCSTAR 1: Final Report on the Collapse of the World Trade Center Building 7, 2008.

[7] T. Gernay, N.E. Khorasani, Recommendations for performance-based fire design of composite steel buildings using computational analysis, J. Constr. Steel Res. 166 (2020) 105906. https://doi.org/10.1016/j.jcsr.2019.105906.

[8] K. McGrattan, S. Hostikka, R. McDermott, J. Floyd, C. Weinschenk, K. Overholt, Sixth edition fire dynamics simulator technical reference guide volume 1 : mathematical model, NIST Spec. Publ. 1018. 1 (2015). https://doi.org/10.6028/NIST.SP.1018-1.

[9] F. McKenna, G. Fenves, M. Scott, OpenSees: Open System for Earthquake Engineering Simulation, (2000).

[10] J. Jiang, A. Usmani, G.-Q. Li, Modelling of Steel-Concrete Composite Structures in Fire Using OpenSees., Adv. Struct. Eng. 17 (2014) 249–264. https://doi.org/10.1260/1369-4332.17.2.249.

[11] J. Jiang, L. Jiang, P. Kotsovinos, J. Zhang, A. Usmani, OpenSEES Software Architecture for the Analysis of Structures in Fire, J. Comput. Civ. Eng. 29 (2015) 04014030. https://doi.org/10.1061/(ASCE)CP.1943-5487.0000305.

[12] J. Jiang, P. Khazaeinejad, A. Usmani, Nonlinear analysis of shell structures in fire using OpenSees, (2012).

[13] M.A. Orabi, A.A. Khan, A. Usmani, An Overview of OpenSEES for Fire, Proc. 1st Eurasian Conf. OpenSEES OpenSEES Days Eurasia. (n.d.) 1–6.

[14] Y. Jiang, Development and application of a thermal analysis framework in OpenSees for structures in fire, The University of Edinburgh, 2012.

[15] T. Kartalis-Kaounis, V.K. Papanikolaou, GiD + OpenSees, (2017).

[16] CIMNE, GiD, (2020).

[17] C. Zhang, J.G. Silva, C. Weinschenk, D. Kamikawa, Y. Hasemi, Simulation Methodology for Coupled Fire-Structure Analysis: Modeling Localized Fire Tests on a Steel Column, Fire Technol. 52 (2016) 239–262. https://doi.org/10.1007/s10694-015-0495-9.

[18] J.C.G. Silva, A. Landesmann, F.L.B. Ribeiro, Fire-thermomechanical interface model for performance-based analysis of structures exposed to fire, Fire Saf. J. 83 (2016) 66–78. https://doi.org/10.1016/j.firesaf.2016.04.007.

[19] K. Prasad, H.R. Baum, Coupled fire dynamics and thermal response of complex building structures, Proc. Combust. Inst. 30 (2005) 2255–2262. https://doi.org/10.1016/j.proci.2004.08.118.

[20] A.A. Khan, M.A. Khan, A. Usmani, X. Huang, S. Bakhtiyari, M.J. Ashtiani, S. Garivani, A.A. Aghakouchak, Framework for Fire Investigation of Tall Buildings: A Case Study of the Plasco Building, Fire Technol. (2021).

[21] K. McGrattan, S. Hostikka, R. McDermott, J. Floyd, C. Weinschenk, K. Overhold, Sixth Edition Fire Dynamics Simulator User ’s Guide (FDS), NIST Spec. Publ. 1019. Sixth Edit (2016). https://doi.org/10.6028/NIST.SP.1019.

[22] NIST, NIST NCSTAR 1: Final Report on the Collaps of the World Trade Centre Towers, 2005.

[23] M.A. Orabi, L. Jiang, A. Usmani, J. Torero, The Collapse of World Trade Center 7: Revisited, in: 11th Int. Confrence Struct. Fire, 2020: pp. 23–33.

[24] B. Merci, T. Beji, Fluid mechanics aspects of fire and smoke dynamics in enclosures, 2016. https://doi.org/10.1201/b21320.

[25] H.R. Baum, M. K.B., R.G. Rehm, Three dimensional simulations of fire plume., in: Fire Saf. Sci. Proc. Fifth Int. Symp., Tsukuba, Japan, 1997: pp. 511–522.

[26] T.G. Ma, J.G. Quintiere, Numerical simulation of axi-symmetric fire plumes: Accuracy and limitations., Fire Saf. Journal, 38,. 38 (2003) 467–492.

[27] G. Rein, J.L. Torero, W. Jahn, J. Stern-Gottfried, N.L. Ryder, S. Desanghere, M. Lázaro, F. Mowrer, A. Coles, D. Joyeux, D. Alvear, J.A. Capote, A. Jowsey, C. Abecassis-Empis, P. Reszka, Round-robin study of a priori modelling predictions of the Dalmarnock Fire Test One, Fire Saf. J. 44 (2009) 590–602. https://doi.org/10.1016/j.firesaf.2008.12.008.

[28] CEN, Eurocode 2 — Design of concrete structures Part 1-1: General rules and rules for buildings, (2015).

[29] CEN, EN 1993-1-2: Design of Steel Structures, Br. Stand. (2006).

[30] V.K.R. Kodur, A.M. Shakya, Effect of temperature on thermal properties of spray applied fire resistive materials, Fire Saf. J. 61 (2013) 314–323. https://doi.org/10.1016/j.firesaf.2013.09.011.

[31] Q. Li, C. Zhang, G.-Q. Li, Symmetric modeling of the experimental thermal actions on a long-span

composite floor beam in a compartment.pdf, (2020).

[32] L. Choe, S. Ramesh, L. Choe, M. Seif, Compartment Fire Experiments on Long-Span Composite-Beams with Simple Shear Connections Part 1 : Experimental Design and Beam Behavior at Ambient Temperature NIST Technical Note 2054 Compartment Fire Experiments on Long-Span Composite-Beams with Simple Sh, 2019.

[33] CEN, General actions-actions on structures exposed to fire, in: EN 1991-1-22002 Eurocode1 Actions Struct., 2002.

[34] L. Jiang, M.A. Orabi, J. Jiang, A. Usmani, Modelling concrete slabs subjected to fires using nonlinear layered shell elements and concrete damage-plasticity material, Eng. Struct. 234 (2021) 111977. https://doi.org/10.1016/j.engstruct.2021.111977.

[35] A. Usmani, J. Zhang, J. Jiang, Y. Jiang, I. May, Using Opensees for Structures in Fire, J. Struct. Fire Eng. 3 (2012) 57–70. https://doi.org/10.1260/2040-2317.3.1.57.

[36] X. Lu, L. Xie, H. Guan, Y. Huang, X. Lu, A shear wall element for nonlinear seismic analysis of super-tall buildings using OpenSees, Finite Elem. Anal. Des. 98 (2015) 14–25. https://doi.org/10.1016/j.finel.2015.01.006.

[37] X. Lu, Y. Tian, S. Cen, H. Guan, L. Xie, L. Wang, A High-Performance Quadrilateral Flat Shell Element for Seismic Collapse Simulation of Tall Buildings and Its Implementation in OpenSees, J. Earthq. Eng. 22 (2018) 1662–1682. https://doi.org/10.1080/13632469.2017.1297269.

[38] L. Jiang, S. Chen, A. Usmani, Feasibility of dimensionally reduced heat transfer analysis for structural members subjected to localised fire, Adv. Struct. Eng. 21 (2018) 1708–1722. https://doi.org/10.1177/1369433218754334.

[39] P.J. Moss, G.C. Clifton, Modelling of the cardington LBTF steel frame building fire tests, Fire Mater. 28 (2004) 177–198. https://doi.org/10.1002/fam.868.

[40] Z. Huang, I.W. Burgess, R.J. Plank, THREE-DIMENSIONAL MODELLING OF TWO FULL-SCALE,FIRE TESTS ON A COMPOSITE BUILDING., Proc. Inst. Civ. Eng. - Struct. Build. 134 (1999) 243–255. https://doi.org/10.1680/istbu.1999.31567.

[41] SFPE, SFPE Handbook of Fire Protection Engineering, 2016. https://doi.org/10.1016/s0379-7112(97)00022-2.

[42] J.G. Quintiere, Fundamental of Fire Phenomena, John Wiley, New York, 2006. https://doi.org/10.1002/0470091150.

[43] A.Y. Elghazouli, B.A. Izzuddin, Realistic Modeling of Composite and Reinforced Concrete Floor Slabs under Extreme Loading. II: Verification and Application, J. Struct. Eng. 9445 (2004) 1562–1569. https://doi.org/10.1061/(ASCE)0733-9445(2004)130.

[44] X. Yu, Z. Huang, I. Burgess, R. Plank, Nonlinear analysis of orthotropic composite slabs in fire, Eng. Struct. 30 (2008) 67–80. https://doi.org/10.1016/j.engstruct.2007.02.013.

[45] X. Yu, Z. Huang, An embedded FE model for modelling reinforced concrete slabs in fire, Eng. Struct. 30 (2008) 3228–3238. https://doi.org/10.1016/j.engstruct.2008.05.004.

[46] A.K. Abu, I.W. Burgess, R.J. Plank, Tensile membrane action of thin slabs exposed to thermal gradients, J. Eng. Mech. 139 (2013) 1497–1507. https://doi.org/10.1061/(ASCE)EM.1943-7889.0000597.

[47] S. Lamont, A.S. Usmani, M. Gillie, Behaviour of a small composite steel frame structure in a “long-cool” and a “short-hot” fire, Fire Saf. J. 39 (2004) 327–357. https://doi.org/10.1016/j.firesaf.2004.01.002.

[48] A.M. Sanad, J.M. Rotter, A.S. Usmani, M.A. O’Connor, Composite beams in large buildings under fire -

Numerical modelling and structural behaviour, Fire Saf. J. 35 (2000) 165–188. https://doi.org/10.1016/S0379-7112(00)00034-5.

[49] E.I. Wellman, A.H. Varma, R. Fike, V. Kodur, Experimental evaluation of thin composite floor assemblies under fire loading, J. Struct. Eng. 137 (2011) 1002–1016. https://doi.org/10.1061/(ASCE)ST.1943-541X.0000451.

[50] A.S. Usmani, N.J.K. Cameron, Limit capacity of laterally restrained reinforced concrete floor slabs in fire, Cem. Concr. Compos. 26 (2004) 127–140. https://doi.org/10.1016/S0958-9465(03)00090-8.

[51] O. Vassart, B. Zhao, FRACOF: Engineering Background, 2011.

[52] Z.N. Yang, Y.L. Dong, W.J. Xu, Fire tests on two-way concrete slabs in a full-scale multi-storey steel-framed building, Fire Saf. J. 58 (2013) 38–48. https://doi.org/10.1016/j.firesaf.2013.01.023.